ChemCatChem

Research Article
doi.org/10.1002/cctc.202101828

Europe
European Chemical
Societies Publishing

www.chemcatchem.org

Structure-Activity Relationships in Highly Active Platinum-Tin MFI-type Zeolite Catalysts for Propane Dehydrogenation

Inés Lezcano-González,[a, b] Peixi Cong,[a, b] Emma Campbell,[a, b] Monik Panchal,[a, b] Miren Agote-Arán,[a, b] Verónica Celorrio,[c] Qian He,[d] Ramon Oord,[e] Bert M. Weckhuysen,[e] and Andrew M. Beale*[a, b]

Pt/Sn-containing MFI zeolites prepared by one-pot hydro-thermal methods are highly active and selective catalysts for propane dehydrogenation. An alternative preparation method is reported alongside an in-depth characterization of Pt and Sn before and after reaction. Pt species dispersed on highly-defective Silicalite-1 show a significantly long catalytic lifetime with an improved coke resistance, but increased Pt–Sn alloying and the (eventual) build-up of carbon leads to deactivation.

Introduction

Crude oil is still the primary source of many platform chemicals for the chemical industry. In particular light olefins, such as ethylene and propylene, typically obtained through naphtha cracking, provide the basic building blocks for the complex molecules that comprise polymers and pharmaceuticals.[1] Non-conventional extraction processes, such as fracking and coal gasification, are providing an increasing supply of cheap alkanes resulting in the USA becoming a net chemicals exporter.[1] However, this has been at the expense of naphtha crackers which has led to a spike in propylene prices,[2] resulting in several chemical companies focusing on alternative MTO/MTH (Methanol-to-Olefins/Hydrocarbons) and PDH (propane dehydrogenation) technologies for its manufacture.[1]

Commercial processes for the catalytic dehydrogenation of light alkanes typically use either supported Cr-based or Pt/Sn-based catalysts, although issues related to the use of Cr (as carcinogenic Cr^{6+} is formed during regeneration), the very high and unstable price of Pt and especially, the fast catalyst deactivation have prompted to search for alternative catalyst formulations. The main problem with existing catalytic technologies is that the inherent acidity of the support (typically γ-Al_2O_3) is well known to promote oligomerization, cyclization and condensation reactions, leading to coke formation. This requires frequent regeneration (combustion), leading to a gradual loss in activity as a result of metal sintering.[1,3,4] Though carbon deposition can be partially mitigated against using promoters (i.e. through reducing support acidity, enhancing coke diffusion and inhibiting side reactions),[1,3,5–7] it is to be noted that some studies have shown that these coke deposits could in fact be necessary, through the blocking of side reactions or even to be catalytically active itself.[8] Besides a limited acidity, a high thermal stability of the support is required due to the harsh hydrothermal conditions used during regeneration, together with a large surface area to allow an optimal distribution of the active sites.[1,2]

Due to their particular properties, zeolites have found use as support for light alkane dehydrogenation catalysts.[9–30] Several studies using Pt-containing MFI-type zeolites with different balancing cations and/or promoters have been published in the literature over the last decades.[9–25] Small Pt clusters within the 10r channels of ZSM-5 zeolite, containing isomorphously substituted Fe^{3+} ions and Na^+ as balancing cations, have been shown to catalyze propane dehydrogenation with higher rates, selectivity and stability than Pt/Sn-Al_2O_3, attributed to the presence of well-dispersed Pt within the zeolite micropores, the

[a] Dr. I. Lezcano-González, P. Cong, Dr. E. Campbell, M. Panchal, Dr. M. Agote-Arán, Prof. A. M. Beale
Department of Chemistry
University College London
20 Gordon Street
London, WC1H 0AJ (UK)
E-mail: a.m.beale@ucl.ac.uk

[b] Dr. I. Lezcano-González, P. Cong, Dr. E. Campbell, M. Panchal, Dr. M. Agote-Arán, Prof. A. M. Beale
UK Catalysis Hub
Research Complex at Harwell
Rutherford Appleton Laboratories
Harwell Science and Innovation Campus
Harwell
Didcot, Oxon, OX11 0FA (UK)

[c] Dr. V. Celorrio
Diamond Light Source Ltd
Harwell Science and Innovation Campus
Didcot OX11 0DE (UK)

[d] Dr. Q. He
Cardiff Catalysis Institute
School of Chemistry
Cardiff University
Cardiff, CF10 3AT (UK)

[e] Dr. R. Oord, Prof. B. M. Weckhuysen
Inorganic Chemistry and Catalysis
Debye Institute for Nanomaterials Science
Utrecht University
Universiteitsweg 99
3584 CG, Utrecht (The Netherlands)

ChemCatChem

Research Article
doi.org/10.1002/cctc.202101828

Chemistry Europe
European Chemical
Societies Publishing

weaker acid sites resulting from framework Fe^{3+} ions (as compared with Al-containing zeolites), and geometric constraints inhibiting the formation of bulky hydrocarbons.[11–12] More recently, it has been shown to be possible to synthesize in one pot siliceous (K)PtSnMFI zeolites that are highly active, selective and stable in the dehydrogenation of propane; utilizing the zeolite shape-selectivity to favor dehydrogenation over oligomerization and the absence of Brønsted sites to mitigate coke formation.[23–25]

In this work we report a variant on the above preparation method, resulting in well-dispersed Pt particles deposited onto silanol defects, generated by basic post-synthesis treatment (see SI for further details; Figures S1–S5 and Tables S1–2), to create similarly a highly active/selective Pt(Sn)MFI-type catalyst which is relatively straightforward to prepare. Detailed characterization has been subsequently performed in order to determine the Pt/Sn species responsible for high performance as well as the evolution of these species that lead to deactivation.

Results and Discussion

The catalytic performance of the zeolite-based samples was evaluated at 600 °C and 1 bar for 10 h and is shown in Figures 1a and 1b. Pt/Silicalite-1 showed higher initial conversions than Pt–Sn/Silicalite-1 (64 vs 42%). This conversion, which is above equilibrium (calculated to be 47–54.6%),[1] is accompanied by a propene selectivity of 54%, the remaining products being mainly methane and ethane (see Figure S6). For comparison, we note the recent work by Liu *et al.* reported conversions as high as 63% with 97% propene selectivity.[23] Over the entire reaction on Pt/Silicalite-1 (see Figures 1a, 1b and S6), both methane and ethane were produced in the same molar concentration – as expected for propane hydrogenolysis, although their selectivity constantly dropped, pointing to the gradual deactivation of the sites responsible for this side reaction. This could be understood in terms of the structure sensitivity of propane hydrogenolysis; i.e. a gradual deactivation of the Pt particles responsible for this side reaction – allegedly the large particles located on the external zeolite surface (*vide infra*),[32] may be taking place during reaction as a result of coke deposition, leading to a decrease in the rate of hydrogenolysis. Interestingly, the trend in product selectivity for Pt/Silicalite-1 completely differs with that previously observed by Iglesias-Juez *et al.* for Pt on Al_2O_3, which showed a high selectivity towards cracking products.[3]

In sharp contrast, a very high selectivity towards propene was observed for Pt/Sn-Silicalite-1 (95%), which showed a fairly stable propane conversion (~40–42%) for 10 h of reaction and very minor amounts of hydrogenolysis products, reflecting the positive effect of Sn on the catalytic performance. Remarkably, the performance is very comparable to what has already been reported and in excess of some of the lab-tested Pt/Sn-Al_2O_3 and industrial catalytic samples (Pt–Sn/$ZnAl_2O_3$) used in the Uhde STAR process, which are known to deactivate (conversions dropping from 37% with selectivity's ~90%) in ~6–7 h.[33]
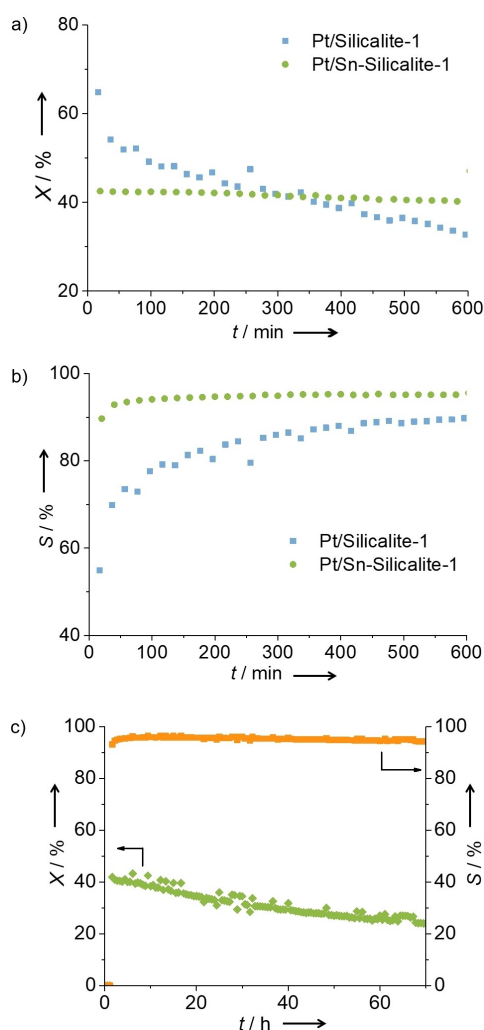

Figure 1. a) Propane conversion and b) propene selectivity during propane dehydrogenation over Pt/Silicalite-1 and Pt/Sn-Silicalite-1 for 10 h, and c) Propane conversion and propene selectivity during propane dehydrogenation over Pt/Sn-Silicalite-1 for 70 h. The reaction temperature and pressure were 600 °C and 1 bar, respectively. WHSV = 3.2 h^{-1}.

In order to further investigate the performance of Pt/Sn-Silicalite-1 over an extended reaction period, an additional test was performed for 70 h (Figure 1c). While a limited drop in propane conversion was observed (from 42 to 24%), propene selectivity remained rather constant, in line with the enhanced lifetime of this catalyst material. In the study by Liu *et al.*[23] a similar trend was seen to take place for a 20 h reaction period, although the conversion remained above equilibrium during the first 5–8 h. We also observe that the calculated deactivation constant for our Pt/Sn-Silicalite-1 catalyst is 0.012 h^{-1}, consistent with that previously reported by Liu *et al.*[24]

To further understand the catalytic behavior of Pt/Sn-Silicalite-1, both fresh and reacted samples were characterized by different methods, so as to gain insight into particle size effects, Pt dispersion, Pt–Sn alloying or the possible formation of coke deposits. High-angle annular dark-field scanning transmission electron microscopy (HAADF-STEM) micrographs of the
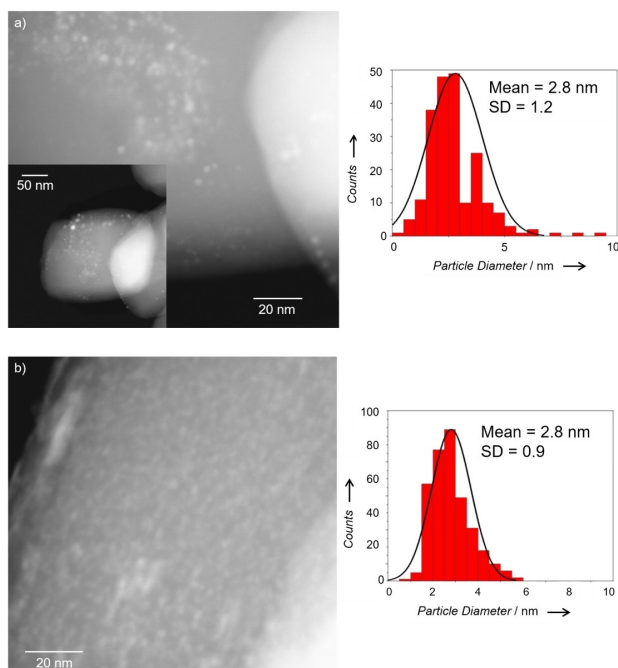
ChemCatChem

Research Article
doi.org/10.1002/cctc.202101828

Chemistry
Europe

European Chemical
Societies Publishing

Figure 2. HAADF-STEM micrographs and corresponding histogram plots of the reduced a) Pt/Silicalite-1 sample, and b) Pt/Sn-Silicalite-1 catalysts.
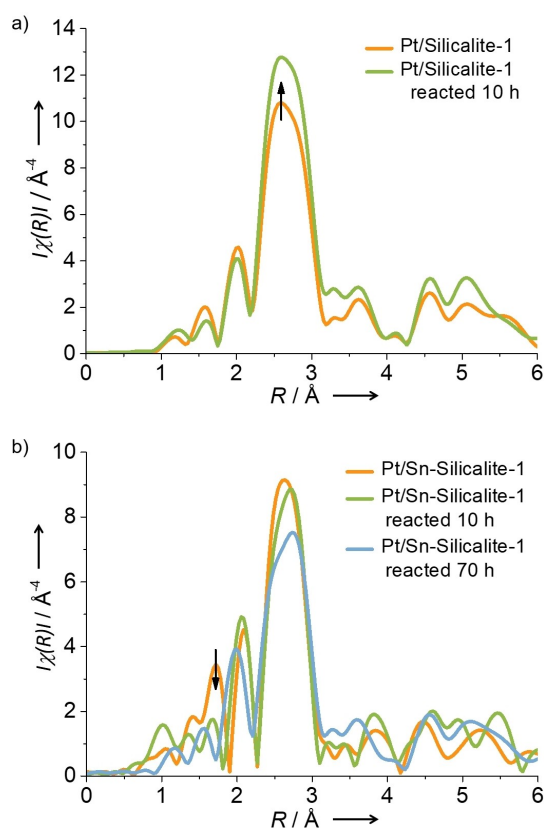

Figure 3. Magnitude of the Fourier Transform (FT) of reduced and reacted a) Pt/Silicalite-1, and b) Pt/Sn-Silicalite-1.

reduced Pt/Silicalite-1 (Figure 2a) evidenced the presence of very small Pt particles, along with minor amounts of larger agglomerates. The accompanying histogram plot suggests particles that can be seen to be ~2.8 nm. Similarly, the HAADF-STEM micrographs of Pt/Sn-Silicalite (Figure 2b) point out to an average particle size of about 2.8 nm, although no large particles could be found on this catalyst material, indicated by a lower standard deviation in the mean particle size. While large particles are likely to be located on the outer shell of the zeolite crystals, sub-nanometer particles are expected to be placed within the zeolite micropores.[23–25] Note however, that due to the low contrast (resulting from the support thickness), ultra-small Pt species are rather difficult to visualize. Electron Dispersive X-ray Spectroscopy (EDS) maps of Pt/Sn-Silicalite-1 are presented in Figure S7.

Volume averaged data was also acquired in the form of X-ray Absorption Spectroscopy (XAS) data. The Pt L_3-edge X-ray near edge structure (XANES) spectra of both Pt-Silicalite-1 and Pt/Sn-Silicalite-1 are shown in Figure S8 and comprise a rising absorption edge larger than that seen for metallic Pt (foil) yet lower than that seen for oxides of Pt (i.e. PtO/PtO_2) and is consistent with the presence of Pt nanoparticles with a degree of oxidic character.[34] In line with the XANES data, the Fourier transforms (FT) of the extended X-ray absorption fine structure (EXAFS) data of both samples (Figure 3) are dominated by a component at 0.275 nm due to Pt—Pt scattering. Interestingly, the Pt/Sn-Silicalite-1 sample possesses a short component at 0.175 nm consistent with a Pt—O contribution not present for the Pt/Silicalite-1 catalyst. This suggests a better dispersion of Pt in Pt/Sn-Silicalite-1 and therefore a more significant inter-action with the zeolite framework.

K-space fitting of the EXAFS data confirmed the presence of nanoparticulate Pt in both samples (see Table 1). The similarity of the average Pt—Pt shell distance for both samples indicates that there is little obvious binary alloying/intermetallic forma-tion in the Pt/Sn-Silicalite-1 sample and is consistent with previous data that has shown such species tend to form after reaction/regeneration.[3,35] Assuming then a segregated-system, the Pt particle size can be determined from the Pt—Pt coordination number.[36] For Pt/Silicalite-1 a coordination num-ber of 7.4, was obtained corresponding to an average (spherical) Pt particle size of 1.1 nm (Table 1).[36] This average size is smaller than the one obtained by HAADF-STEM, as by EXAFS is now possible to account for the ultra-small particles difficult to observe by HAADF-STEM. Interestingly, for Pt—Sn/

Table 1. Pt—Pt coordination number and average particle size of Pt/Silicalite-1and Pt/Sn-Silicalite-1 catalysts after *in situ* reduction under H_2 flow for 1 h at room temperature and after propane dehydrogenation reaction at 600 °C and 1 bar (WHSV = 3.2 h^{-1}).

	Reduced		Reacted	
	CN_{Pt-Pt}	Part. size [nm]	CN_{Pt-Pt}	Part. size [nm]
Pt/Silicalite-1[a]	7.4	1.1	8.7	2.0
Pt/Sn-Silicalite-1[a]	6.1	0.7	5.6	0.6
Pt/Sn-Silicalite-1[b]			5.0	0.5
[a] Sample reacted for 10 h. [b] Sample reacted for 70 h.				

ChemCatChem

Research Article
doi.org/10.1002/cctc.202101828

Chemistry
Europe
European Chemical
Societies Publishing

Silicalite-1 the coordination number is significantly smaller (~6.1) and equates to a particle size of ~0.7 nm (notwithstanding the error associated with the CN to be ~10–20%). This is of the order of the pore openings of the MFI structure (~5.6 Å) and is suggestive that the majority of Pt species to be clustered and likely confined within the zeolite structure. The larger average size obtained by EXAFS for Pt/Silicalite-1 can be explained by the presence of larger aggregates in this sample (as per the HAADF-STEM results).

Sn K-edge XAS measurements were also performed (Figure S9). The XANES spectrum of the reduced Pt/Sn-Silicalite-1 sample (Figure S9a) resembles that of a SnO_2 reference, suggesting that the Sn sites are present as Sn(IV) species. We note that, as previous studies have shown, it is difficult to unambiguously determine the coordination state of Sn (IV).[37] However, when compared to bulk SnO_2, which contains octahedrally coordinated Sn(IV), the lower intensity observed for both the Sn–O contribution in the FT and the main edge in the XANES indicates differences in the Sn coordination environment, due to the presence of at least some Sn(IV) species in tetrahedral coordination.[38] The presence of higher R-space features between 3–4 Å in the EXAFS FT (Figure S9b) confirms that some octahedral Sn (IV) is still present in the form of SnO_2 clusters. We propose tetrahedral Sn (IV) sites to occupy framework positions due to the incorporation of Sn into the framework vacancies. Furthermore, it appears that this Sn (IV) incorporation leads to better Pt dispersion, with isomorphously-substituted Sn acting as a Lewis acid site onto which Pt-amines may complex, favoring an enhanced Pt dispersion.

In order to investigate whether Pt sintering occurred during reaction, the spent zeolite catalysts were further characterized by XAS (Figure 3 and S8–9, and Tables 1 and S3). The Fourier transform (FT) of the Pt/Silicalite-1 catalyst sample showed an increased intensity of the Pt–Pt contribution (Figure 3), indicating the presence of larger Pt particles (~2 nm) after reaction (Table 1).[36] Importantly, no significant sintering was detected for the spent Pt/Sn-Silicalite-1 catalysts after both 10 h and 70 h of reaction (Figure 3 and Table 1). The FT for the reduced and reacted catalyst samples are remarkably similar and suggest that, in comparison, the presence of Sn affords stability of the Pt species. Both the lack of a short Pt–O component in the FT and the decreased rising absorption edge intensity in the Pt L_3 XANES data for the reacted Pt/Sn-Silicalite-1 sample (Figure S8) suggest that Pt is more reduced than at the beginning. However a shift in the rising absorption edge towards higher energies is also observed and previously been attributed to Sn withdrawing electron density from Pt, resulting from an electronic interaction between Pt and Sn.[3] Importantly, no differences in the Pt L_3 XANES spectra are observed between 10 and 70 h of reaction (Figure S8), suggesting that the changes mentioned above occur over the first 10 h. The Fourier transform data after 10 h of reaction shows only a small change in the intensity ratio of the two peaks between 2–3 Å suggesting some (minor) degree of Pt–Sn alloying (Figure 3).[3,39] Furthermore, a red shift in the position of the Sn K-edge XANES of the reacted Pt/Sn-Silicalite-1 catalysts (Figure S9a) and a reduced

Sn–O coordination number (Table S3) are observed, also consistent with a partial reduction of Sn species.

Thermogravimetric analysis (TGA) was performed to analyze the carbon deposits formed on the catalyst surface during reaction. As shown in Table 2, the amount of carbon present on both Pt- and Pt/Sn-Silicalite-1 samples after 10 h and 70 h of reaction was significantly lower than that formed on either Pt/H-ZSM-5 (see section 6 in the SI for further details; Figures S10-S12 and Table S4) or Al_2O_3-based catalysts (i.e. 2 to 12 times lower), evidencing the higher coke resistance of the Silicalite-supported catalysts. Interestingly, the quantity of coke on Pt/Sn-Silicalite-1 after 10 h was greater than on Pt/Silicalite-1 (although with comparable combustion temperatures, indicative of deposits of similar nature), showing no clear correlation with the catalytic activity. Similar results were recently reported for both Pt/Al_2O_3 and Pt/Sn–Al_2O_3 catalysts, leading to the proposal that deactivation does not occur solely due to the blockage of the metal sites by carbon.[4] It is known that coke formation is structure-sensitive, and that large Pt particles are needed to catalyze its formation.[5,40] In view of the absence of Brønsted sites promoting the formation of coke precursors, it is therefore, reasonable to assume that the carbon deposits produced on both Pt/Silicalite-1 and Pt/Sn-Silicalite-1 are mainly formed over the large Pt particles located at the outer zeolite surface. Accordingly, the differences observed in the amount of deposited carbon on these samples probably arise from a combination of different effects, such as the size of Pt particles, the extent of sintering and/or the likelihood of coke precursors migrating to the zeolite support, although from the data obtained it is difficult to drawn definitive conclusions. Nevertheless, considering the low amount of carbon present on Pt/Silicalite-1, it can be suggested that the deactivation of this catalyst is directly related to Pt agglomeration - as previously seen by XAFS, leading to a non-optimal variation in particle size.

The deposition of carbon over the large Pt particles will in turn, explain the trends in propene selectivity observed for these materials; as for coking, propane hydrogenolysis is a structure-sensitive reaction,[1,32] so the formation of coke over the large Pt particles will certainly inhibit this side reaction, leading to a decrease in the selectivity towards both ethane and methane, as indeed shown above. Additionally, the

Table 2. Carbon weight loss of zeolite-based and Al_2O_3-based catalyst materials as determined by TGA after propane dehydrogenation reaction at 600 °C and 1 bar (WHSV = 3.2 h^{-1}).

	Weight loss [wt%]	T_{comb} [°C]	Ref.
Pt/Sn-Silicalite-1[a]	3.1	534	*This work*
Pt/Sn-Silicalite-1[b]	5.7	566	*This work*
Pt/Silicalite-1[a]	1.1	502	*This work*
Pt/H-ZSM-5[a,c]	12.1	556 (sh.615)	*This work*
Pt/Sn-Al_2O_3[d]	10.5	505	[4]
Pt/Al_2O_3[d]	6.2	440	[4]

[a] Reaction carried out for 10 h. [b] Reaction carried out for 70 h. [c] Catalyst sample prepared for comparison purposes, characterization and activity data provided in section 6 in the SI. [d] Reaction carried out for 6 h.

ChemCatChem

Research Article
doi.org/10.1002/cctc.202101828

**Chemistry
Europe**

European Chemical
Societies Publishing

presence of very small particles within the confined environment of Silicalite-1 will favor dehydrogenation over other side reactions; both geometric constraints and the lack of Brønsted acid sites will inhibit chain growth and cyclization reactions responsible for the formation of coke precursors, accounting for the exceptional coke resistance of these catalyst materials. Indeed, as compared to standard Pt/Sn-Al$_2$O$_3$, the Pt/Sn-Silicalite-1 catalyst leads to a c.a. 2-fold decrease in the amount of deposited carbon, even after more than 10-times longer reaction times (6 vs. 70 h), thereby requiring less frequent oxidative regeneration treatments known to inevitably trigger a gradual deactivation.

Conclusions

Small platinum particles dispersed on a highly-defective Silicalite-1 zeolite containing Sn as a promotor are able to effectively catalyze the dehydrogenation of propane with very high propene selectivity and yield but perhaps more importantly, with exceptional coke resistance. This catalyst material was thoroughly characterized by a number of techniques, including XAFS, suggesting the presence of very small particles located within the MFI micropores and isomorphously substituted Sn(IV) species. It is believed that both framework Sn(IV) and silanol defect groups, together with geometric constraints within the zeolite micropores, help to maintain a good Pt dispersion. Importantly, this catalyst material exhibits a remarkable coke resistance, leading to a very significant decrease in the amount of coke formed as compared to standard Pt/Sn-Al$_2$O$_3$ catalysts. This can be directly related to the absence of strong acid sites on the catalyst support; silanol groups along with framework Sn sites are instead used to enhance Pt dispersion, likely functioning as anchoring sites for Pt. Despite the limited accumulation of coke, a gradual catalyst deactivation is observed with time on stream, which can also be attributed to increased Pt—Sn alloying during reaction (as pointed by the XAFS data), initially thought to occur during the catalyst regeneration stage.[3]

While the approach here used can further be explored to develop coke resistant catalyst materials for a large number of industrial applications, the versatility and tunability of the preparation method make these materials ideal candidates to be used as model systems for the dehydrogenation of light alkenes, allowing to gain a better understanding into particle size effects, influence of promotors or support acidity, among others, and thereby, aiding in the design of materials with improved performance. Within this context, it has to be noted that while synthetic strategies should also aim to prevent alloy formation – as pointed by our data, this is certainly a very challenging aspect in catalyst design.

Experimental Section

Catalyst Preparation

Silicalite-1 zeolite was synthesized following the method previously reported by Kragten et al.,[41] and subsequently submitted to a basic treatment with ethylenediamine; this treatment is known to generate additional silanol groups (T-site vacancies or defects) through the removal of framework silicon,[42] serving as anchoring sites for metal species.[43] Typically, 1 g of Silicalite-1 calcined at 550 °C for 12 h was impregnated with 2 g of ethylenediamine and heated in a stainless steel autoclave at 120 °C for 3 h. The final catalyst was thoroughly washed with deionized water and subsequently dried at 120 °C overnight. Zeolite NH$_4$-ZSM-5 (Si/Al = 15) produced by Zeolyst is commercially available (CBV3024E). The proton form was obtained by calcination in static air at 550 °C for 8 h.

0.5 wt % Pt/Silicalite-1 and 0.5 wt % Pt/H-ZSM-5 were prepared via incipient wetness impregnation, using an aqueous solution of Pt(NH$_3$)$_4$(NO$_3$)$_2$. 0.5 wt% Pt- 1.5 wt% Sn/Silicalite-1 was prepared by incipient wetness impregnation with Pt(NH$_3$)$_4$(NO$_3$)$_2$, followed by solid-state ion exchange with appropriate amounts of Sn-(CH$_3$CO$_2$)$_4$.[37,44,45] After a drying step at 120 °C for 8 h, the zeolite samples were calcined in static air at 350 °C for 2 h using a heating rate of 2 °C.min^{-1}.

Characterization Methods

XRD patterns of the parent and post-treated Silicalite-1 samples were recorded on a Rigaku SmartLab Diffractometer equipped with a Cu Kα radiation source (λ = 1.5406 Å). The measurements were performed from 5–55° using a step size 0.01° at 0.5°/min and spinning 180°/min. Diffuse reflectance infrared Fourier transform spectroscopy (DRIFTS) data were recorded on an Agilent Carey 680 FT-IR spectrometer using the Praying Mantis Diffuse Reflectance accessory from Harrick Scientific. Each sample was dried prior to the measurement by heating to 500 °C for 1 h under He flow. After dehydration, the sample was cooled to 150 °C under He before spectra collection. ^{1}H solid-state Nuclear Magnetic Resonance (NMR) spectra were recorded at a static magnetic field strength of 9.4 T (v$_0$ = 400.16 MHz) on a Bruker Avance III console. The sample was dehydrated at 350 °C overnight under vacuum and subsequently transferred into a rotor under dry atmosphere. The ^{1}H NMR spectrum was acquired with a widebore Bruker 4 mm BB/1H WVT MAS probe spinning the sample at 10 kHz, and using recycle delays of 4 s. The spectrum was referenced to d16 adamantane at 1.73 ppm. Temperature programmed desorption of ammonia (NH$_3$-TPD) was performed using an AutoChem II 2920 micromeritics instrument equipped with a moisture trap and a thermo-conductivity detector. Samples were first activated in pure N$_2$ at 550 °C for 30 min. The sample was then cooled down to 100 °C for ammonia adsorption, run by flowing 1% NH$_3$/N$_2$ until saturation (~1 h), followed by a flow of pure N$_2$ for 2 h to remove physisorbed ammonia. Ammonia desorption was carried out by increasing the temperature, using a heating rate of 10 °C/min. XRD, DRIFTS, NMR and NH$_3$-TPD data are provided in the Supporting Information.

Pore volumes and Brunauer-EmmettTeller (BET) surface areas were determined by nitrogen sorption measurements using a Quadrasorb EVO QDS-30 instrument. The chemical analysis was performed by microwave plasma-atomic emission spectrometry (MP-AES, Agilent 4100 instrument). Thermogravimetric analysis (TGA) measurements were carried out in a TA Q50 instrument. Samples were heated up to 950 °C using a ramp of 5 °C/min under air flow. The crystal size and morphology of the samples was analyzed by scanning electron microscopy (SEM) using a JSM-6610LV micro-

ChemCatChem

Research Article
doi.org/10.1002/cctc.202101828

**Chemistry
Europe**
European Chemical
Societies Publishing

scope. N_2 sorption, SEM and MP-AES data are provided in the Supporting Information.

Particle Size Distribution was evaluated using a JEOL JEM 2800 (Scanning) TEM at 200 kV with a C2 (μm) 70 and 40. Micrographs were captured through High angle annular dark-field (HAADF) and Bright Field (BF) imaging in scanning mode with the used of an off-axis annular detector. 435 particles were measured to determine average size. Secondary electron signals were acquired simultaneously with other STEM images, providing topological information of the samples. Prior to the measurements, the as-prepared catalyst samples were *in situ* reduced under H_2 for 1 h at RT.

X-ray absorption spectroscopy (XAS) measurements were carried out at the B18 beamline at Diamond Light Source in Harwell, United Kingdom. The storage beam energy was 3 GeV and the ring current 200 mA. Data were collected at the Sn K-edge (29200 eV) at the Pt L_3-edge (11564 eV) in fluorescence mode with a fast scanning Si (3 1 1) and Si (1 1 1) double crystal monochromators, respectively. All catalyst samples were pressed into pellets, with the amount of sample optimized to obtain a suitable edge step. Prior to the measurements, the as-prepared catalyst samples were *in situ* reduced under H_2 for 1 h at RT, using an *in situ* cell designed for pellet samples which allows measuring in fluorescence mode. For these zeolite samples, data were collected in H_2 atmosphere. XAS data analysis was performed using the Demeter software package.[46,47] The X-ray absorption fine structure (EXAFS) fitting to model spectra was done using an amplitude reduction factor of ~0.91, which was obtained by fitting the foil reference to crystallographic data from the ICSD database. K range values used in the fitting were between 3 and 11 Å^{-1} whereas the R range spanned 1 to 3 Å were used. The respective edge positions were taken as the energy at half-step height and the Fourier transformed (FT) EXAFS data presented are phase corrected.

Catalytic testing

Catalytic tests were performed at 600 °C for 10 h in a packed bed reactor loaded with 0.3 g of sample. For the Pt/Sn-Silicalite-1 sample, an additional stability test was performed, carrying the reaction for 70 h. Prior to the experiment, the catalyst was activated under H_2 (9 ml/min) by increasing the temperature up to 600 °C (10 °C.min^{-1}). After flushing the reactor with He, propane dehydrogenation was performed at 600 °C and atmospheric pressure using a flow of pure propane (9 ml/min; WHSV = 3.2 h^{-1}). Online analysis of the reaction products was performed using an Interscience Compact GC, equipped with an Rtx-wax and Rtx-1 column in series and an Rtx-1, Rt-TCEP and Al_2O_3/Na_2SO_4 in series, both connected to their own FID detector. The permanent gasses were analyzed using a Shincarbon column connected to a TCD detector. The deactivation constant was estimated according to the formula previously presented in the work of Liu *et al.*[24]

Conflict of Interest

The authors declare no conflict of interest.

Data Availability Statement

The data that support the findings of this study are available from the corresponding author upon reasonable request.

[1] J. J. H. B. Sattler, J. Ruiz-Martinez, E. Santillan-Jimenez, B. M. Weckhuysen, *Chem. Rev.* **2014**, *114*, 10613–10653.
[2] J. C. Bricker, *Top. Catal.* **2012**, *55*, 1309–1314.
[3] A. Iglesias-Juez, A. M. Beale, K. Maaijen, T. C. Weng, P. Glatzel, B. M. Weckhuysen, *J. Catal.* **2010**, *276*, 268–279.
[4] H. N. Pham, J. J. H. B. Sattler, B. M. Weckhuysen, A. K. Datye, *ACS Catal.* **2016**, *6*, 2257–2264.
[5] H. Lieske, A. Sárkány, J. Völter, *Appl. Catal.* **1987**, *30*, 69–80.
[6] J. Shen, J. M. Hill, R. M. Watwe, B. E. Spiewak, J. A. Dumesic, *J. Phys. Chem. B* **1999**, *103*, 3923–3934.
[7] R. D. Cortright, J. A. Dumesic, *J. Catal.* **1995**, *157*, 576–583.
[8] C. H. Collett, J. McGregor, *Catal. Sci. Technol.* **2016**, *6*, 363–378.
[9] S. A. I. Barri, US 4,665,267, **1987**.
[10] S. A. I. Barri, R. Tahir, US 5,126,502, **1992**.
[11] T. Waku, J. A. Biscardi, E. Iglesia, *Chem. Commun.* **2003**, *0*, 1764.
[12] T. Waku, J. A. Biscardi, E. Iglesia, *J. Catal.* **2004**, *222*, 481–492.
[13] X. Li, E. Iglesia, *Chem. Commun.* **2008**, *0*, 594–596.
[14] P. L. De Cola, R. Gläser, J. Weitkamp, *Appl. Catal. A* **2006**, *306*, 85–97.
[15] M. Santhosh Kumar, A. Holmen, D. Chen, *Microporous Mesoporous Mater.* **2009**, *126*, 152–158.
[16] Y. Zhang, Y. Zhou, H. Liu, Y. Wang, Y. Xu, P. Wu, *Appl. Catal. A* **2007**, *333*, 202–210.
[17] Y. Zhang, Y. Zhou, L. Huang, M. Xue, S. Zhang, *Ind. Eng. Chem. Res.* **2011**, *50*, 7896–7902.
[18] Y. Zhang, Y. Zhou, M. Tang, X. Liu, Y. Duan, *Chem. Eng. J.* **2012**, *181–182*, 530–537.
[19] W. Wannapakdee, T. Yutthalekha, P. Dugkhuntod, K. Rodponthukwaji, A. Thivasasith, S. Nokbin, S. Witoon, S. Pengpanich, C. Wattanakit, *Catal.* **2019**, *9*, 174.
[20] R. Ryoo, J. Kim, C. Jo, S. W. Han, J.-C. Kim, H. Park, J. Han, H. S. Shin, J. W. Shin, *Natur* **2020**, *585*, 221–224.
[21] X. Zhu, X. Wang, Y. Su, *Catal. Sci. Technol.* **2021**, *11*, 4482–4490.
[22] J. Zhu, R. Osuga, R. Ishikawa, N. Shibata, Y. Ikuhara, J. N. Kondo, J. Ogura, J. Yu, T. Wakihara, Z. Liu, T. Okubo, *Angew. Chem.* **2020**, *132*, 19837–19842; *Angew. Chem. Int. Ed.* **2020**, *59*, 19669–19674.
[23] L. Liu, M. Lopez-Haro, C. W. Lopes, C. Li, P. Concepcion, L. Simonelli, J. J. Calvino, A. Corma, *Nat. Mater.* **2019**, *18*, 866–873.
[24] L. Liu, M. Lopez-Haro, C. W. Lopes, S. Rojas-Buzo, P. Concepcion, R. Manzorro, L. Simonelli, A. Sattler, P. Serna, J. J. Calvino, A. Corma, *Nat. Catal.* **2020**, *3*, 628–638.
[25] L. Liu, M. Lopez-Haro, C. W. Lopes, D. M. Meira, P. Concepcion, J. J. Calvino, A. Corma, *J. Catal.* **2020**, *391*, 11–24.
[26] L. Qi, M. Babucci, Y. Zhang, A. Lund, L. Liu, J. Li, Y. Chen, A. S. Hoffman, S. R. Bare, Y. Han, B. C. Gates, A. T. Bell, *J. Am. Chem. Soc.* **2021**, *143*, 21364–21378.
[27] Z. Xu, Y. Yue, X. Bao, Z. Xie, H. Zhu, *ACS Catal.* **2019**, *10*, 818–828.

[28] Y. Yue, J. Fu, C. Wang, P. Yuan, X. Bao, Z. Xie, J. M. Basset, H. Zhu, *J. Catal.* **2021**, *395*, 155–167.

[29] L. Xie, Y. Chai, L. Sun, W. Dai, G. Wu, N. Guan, L. Li, *J. Energy Chem.* **2021**, *57*, 92–98.

[30] D. Zhao, X. Tian, D. E. Doronkin, S. Han, V. A. Kondratenko, J. D. Grunwaldt, A. Perechodjuk, T. H. Vuong, J. Rabeah, R. Eckelt, U. Rodemerck, D. Linke, G. Jiang, H. Jiao, E. V. Kondratenko, *Natur* **2021**, *599*, 234–238.

[31] Y. Zhang, M. Xue, Y. Zhou, H. Zhang, W. Wang, Q. Wang, X. Sheng, *RSC Adv.* **2016**, *6*, 29410–29422.

[32] R. D. Cortright, J. A. Dumesic, *J. Catal.* **1994**, *148*, 771–778.

[33] H. Z. Wang, L. L. Sun, Z. J. Sui, Y. A. Zhu, G. H. Ye, D. Chen, X. G. Zhou, W. K. Yuan, *Ind. Eng. Chem. Res.* **2018**, *57*, 8647–8654.

[34] M. D. Hall, G. J. Foran, M. Zhang, P. J. Beale, T. W. Hambley, *J. Am. Chem. Soc.* **2003**, *125*, 7524–7525.

[35] H. Verbeek, W. M. H. Sachtler, *J. Catal.* **1976**, *42*, 257–267.

[36] A. M. Beale, B. M. Weckhuysen, *Phys. Chem. Chem. Phys.* **2010**, *12*, 5562.

[37] C. Hammond, D. Padovan, A. Al-Nayili, P. P. Wells, E. K. Gibson, N. Dimitratos, *ChemCatChem* **2015**, *7*, 3322–3331.

[38] K. M. H. Mohammed, A. Chutia, J. Callison, P. P. Wells, E. K. Gibson, A. M. Beale, C. R. A. Catlow, R. Raja, *J. Mater. Chem. A* **2016**, *4*, 5706–5712.

[39] A. G. Mckale, B. W. Veal, A. P. Paulikas, S.-K. Chan, G. S. Knapp, *Phys. Rev. B* **1988**, *38*, 10919–10921.

[40] J. Wu, Z. Peng, A. T. Bell, *J. Catal.* **2014**, *311*, 161–168.

[41] D. D. Kragten, J. M. Fedeyko, K. R. Sawant, J. D. Rimer, D. G. Vlachos, R. F. Lobo, M. Tsapatsis, *J. Phys. Chem. B* **2003**, *107*, 10006–10016.

[42] Y. Bu, Y. Wang, Y. Zhang, L. Wang, Z. Mi, W. Wu, E. Min, S. Fu, *Catal. Commun.* **2007**, *8*, 16–20.

[43] N. A. Grosso-Giordano, A. J. Yeh, A. Okrut, D. J. Xiao, F. Grandjean, G. J. Long, S. I. Zones, A. Katz, *Chem. Mater.* **2017**, *29*, 6480–6492.

[44] C. Hammond, S. Conrad, I. Hermans, *Angew. Chem. Int. Ed.* **2012**, *51*, 11736–11739; *Angew. Chem.* **2012**, *124*, 11906–11909.

[45] Patrick Wolf, Ceri Hammond, Sabrina Conrad, Ive Hermans, *Dalton Trans.* **2014**, *43*, 4514–4519.

[46] M. Newville, *J. Synchrotron Radiat.* **2001**, *8*, 322–324.

[47] B. Ravel, M. Newville, *J. Synchrotron Radiat.* **2005**, *12*, 537–541.